European Journal of Physics

Singularity in the laboratory frame angular distribution derived in two-body scattering theory

IOP PUBLISHING EUROPEAN JOURNAL OF PHYSICS

Eur. J. Phys. **30** (2009) 403–416 doi:10.1088/0143-0807/30/2/019

Singularity in the laboratory frame angular distribution derived in two-body scattering theory

Frank Dick[1] **and John W Norbury**[2]

[1] Worcester Polytechnic Institute, Worcester, MA 01609, USA
[2] NASA Langley Research Center, Hampton, VA 23681-2199, USA

E-mail: fdick@wpi.edu and john.w.norbury@nasa.gov

Received 23 October 2008, in final form 8 January 2009
Published 18 February 2009
Online at stacks.iop.org/EJP/30/403

Abstract

The laboratory (lab) frame angular distribution derived in two-body scattering theory exhibits a singularity at the maximum lab scattering angle. The singularity appears in the kinematic factor that transforms the centre of momentum (cm) angular distribution to the lab angular distribution. We show that it is caused in the transformation by the funnelling of a range of cm scattering angles into a much smaller range of lab angles. Correct treatment of this singularity is important when transforming angular distributions from the cm or projectile frame to the lab frame.

1. Introduction

The transformation of angular distributions, i.e. angular differential cross sections, from one reference frame to another, is essential in a variety of applications. For example, angular differential cross sections are often more easily calculated in the centre of momentum (cm) frame, but need to be transformed to the laboratory (lab) frame of reference in order to compare to measurements made in the lab frame. Another application involves radiation transport codes, which require cross sections expressed in the lab frame. When one transforms the angular distribution for two-body scattering from the cm to the lab frame, a singularity arises in the lab frame angular distribution. Given the fundamental importance of this phenomenon, it is surprising that this is only sparsely discussed in the literature. The aim of this paper is to present a thorough discussion of the methods involved in dealing with this singularity.

The simplest form of scattering involves two-body interactions with the production of two final state particles. In this paper, we limit our discussion to two-body interactions where two particles, labelled 1 and 2, interact to produce final state particles 3 and 4, described symbolically by $1 + 2 \rightarrow 3 + 4$. Three commonly used reference frames are the projectile,

centre of momentum (cm) and target frames. The target frame is often deemed the laboratory (lab) frame, since the target is usually stationary in the laboratory.

In collider beam experiments, involving particles of equal but opposite momentum, the experiment is performed and analysed expeditiously in the cm frame. In experiments involving a particle beam and a stationary target, the lab frame is a natural choice.

The notation used throughout this paper is as follows. Variables in the lab frame are given a subscript l, as in x_l, and variables in the cm frame are given a subscript c, as in x_c.

In the cm frame, the energy of a final state particle is constant over all possible cm scattering angles, $0 \leqslant \theta_c \leqslant \pi$. This is not so in the lab frame, where the energy varies with the lab angle, and where particles of two different energies can scatter into the same angle [1, p 402]. Another feature found in the lab frame is the narrowed range of a scattering angle when the scattered particle masses differ [2, p 100]. For the heavier particle, the range is bounded by the maximum scattering angle $\theta_{l,\max} < \pi/2$, which is determined by the masses and the energy of interaction. We focus on another feature that accompanies the appearance of the maximum scattering angle, namely a *singularity* in the lab angular distribution located at $\theta_{l,\max}$ [2, p 100].

The transformation of angular distributions from the cm to the lab frame is important in illustrating the use of Lorentz and Galilean kinematic transformations. Subsequently, it is discussed in many references concerning classical and quantum mechanics, and nuclear and particle physics [2–30]. The singularity appears in the kinematic factor that arises in the transformation of the distribution from the cm frame to the lab frame, and appears for both the non-relativistic and relativistic cases. It is therefore surprising that the singularity receives no mention in standard discussions of cm to lab transformation of angular differential cross sections [2–30]. The only discussion that we could find in the physics literature was a brief mention in [2, p 100], [3, p 28] and [4, pp 133–4]. A complete treatment of the problem is not given. The purpose of the present paper is to provide such a treatment, which is basic to methods in nuclear and particle physics. We derive the lab angular distribution and demonstrate the presence of the singularity. We relate the existence of the singularity to the nature of the mapping of cm to lab angles. We characterize the singularity in an inelastic scattering process, and we discuss its signature as seen by a macroscopic detector.

The results presented in this paper will be of use to a broad audience. Advanced undergraduates and beginning graduate students will find a thorough, unified treatment of both non-relativistic and relativistic transformations required in calculating angular distributions in both the centre of momentum and lab frames. They will also be introduced to the use of Mandelstam variables. The teacher and general physicist will find a unified treatment of the singularities involved in both the non-relativistic and relativistic transformations of angular distributions. The teacher needs to know about this if these singularities are 'discovered' by sufficiently advanced students. The specialist will find these results useful in practical calculations, such as when lab angular distributions are required by radiation transport codes that require correct treatment of the singularities. The singularity results presented here are not widely available in the literature.

The relevance to physics education is the following. Transformation of the non-relativistic angular distribution from the centre of momentum to the lab frame is a standard lesson in undergraduate and graduate classical and quantum mechanics courses. We provide a thorough discussion of the singularity that is involved in this transformation, which is not widely discussed. Advanced undergraduate and beginning graduate students, as well as teachers, will naturally want to know about the relativistic extension of these results. We discuss the entire problem from the relativistic viewpoint, showing clearly how the relativistic features compare to the non-relativistic features. Such a unified treatment is pedagogically useful.

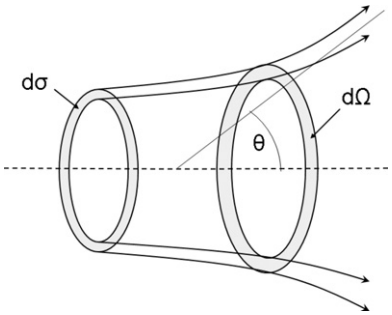

Figure 1. dN is the number of particles incident on $d\sigma$ and scattered into $d\Omega$ per unit time. Adapted from [5].

2. Angular distributions

Following [5], the angular distribution, or angular differential scattering cross section $d\sigma/d\Omega$, is defined as

$$\frac{d\sigma}{d\Omega} = \frac{1}{I}\frac{dN}{d\Omega} \tag{1}$$

$$d\Omega = \sin\theta\, d\theta\, d\phi, \tag{2}$$

where dN is the number of particles incident upon $d\sigma$, the differential element of cross section (figure 1), and scattered into solid angle $d\Omega$, per unit time. The solid angle $d\Omega$ is measured with respect to the origin of the chosen reference frame. The beam intensity I is the number of incident particles per unit area per unit time. The angles θ and ϕ define the scattering direction; θ is the angle between the initial and final lines of motion of the scattered particle and ϕ is the azimuthal angle about the initial line of motion. From figure 1, the differential element of area $d\sigma$ is the same in both the cm and the lab frames, so that

$$d\sigma_c = \frac{d\sigma}{d\Omega_c}\, d\Omega_c = d\sigma_l = \frac{d\sigma}{d\Omega_l}\, d\Omega_l, \tag{3}$$

and by equation (2), with equivalence of the azimuthal angles, $d\phi_c = d\phi_l$, we have

$$\frac{d\sigma}{d\Omega_l} = \left|\frac{d(\cos\theta_c)}{d(\cos\theta_l)}\right| \frac{d\sigma}{d\Omega_c}. \tag{4}$$

The absolute value brackets ensure that $d\sigma/d\Omega_l$ is positive definite. Expressions for the kinematic factor,

$$f \equiv \left|\frac{d(\cos\theta_c)}{d(\cos\theta_l)}\right|, \tag{5}$$

can be derived for both non-relativistic and relativistic scattering, once the relation between the cm and lab scattering angles, θ_c and θ_l, is known. This is done in the following two sections.

3. Non-relativistic scattering

For simplicity, consider elastic scattering in which the colliding particles retain their identities, so that $1 + 2 \rightarrow 1 + 2$. Let particle 1 be the projectile and particle 2 be the target, and consider

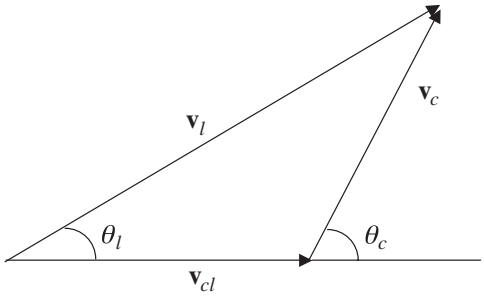

Figure 2. Transformation of velocity from the cm to the lab frame. Adapted from [5].

the scattering of the projectile. The relation between the lab and cm scattering angles, θ_l and θ_c, of the scattered particle is obtained by performing a coordinate transformation of the velocity of the scattered particle from the cm frame to the lab frame. In non-relativistic scattering, the speeds of the interacting particles are small compared to the speed of light c, in both the cm and lab frames. Thus, for the speed v_c of the scattered particle in the cm frame, we have $v_c/c \ll 1$. Furthermore, the speed v_{cl} of the cm frame with respect to the lab frame is small so that $v_{cl}/c \ll 1$. Consequently, the relativistic transformation of velocities reduces to the non-relativistic (Galilean) transformation,

$$\mathbf{v}_l = \frac{\mathbf{v}_c + \mathbf{v}_{cl}}{1 + (\mathbf{v}_c \cdot \mathbf{v}_{cl})/c^2} \simeq \mathbf{v}_c + \mathbf{v}_{cl}, \tag{6}$$

where $\mathbf{v}_l$ is the velocity of the scattered particle in the lab frame. From figure 2, it can be seen that the Galilean transformation [2] of the velocity of the scattered particle yields

$$v_c \cos\theta_c + v_{cl} = v_l \cos\theta_l \tag{7}$$

$$v_c \sin\theta_c = v_l \sin\theta_l, \tag{8}$$

where v is the magnitude of $\mathbf{v}$. Eliminating v_l leads to

$$\tan\theta_l = \frac{\sin\theta_c}{\alpha + \cos\theta_c}, \tag{9}$$

with

$$\alpha \equiv \frac{v_{cl}}{v_c}. \tag{10}$$

Goldstein [6, equation (3.107)] gives an expression identical to equation (9) with α replaced by ρ:

$$\rho = \frac{\mu}{m_2}\frac{v_0}{v_1'}, \tag{11}$$

where $\mu \equiv \frac{m_1 m_2}{m_1 + m_2}$ is the reduced mass and m_1 and m_2 are the masses of the projectile (scattered) particle and target particle, respectively. Also, v_0 is the relative speed of the particles before the collision and v_1' is the speed of the scattered particle in the cm frame. It can be shown that $\alpha = \rho$.

As discussed by Jackson [1], the cm angle, θ_c, can range from 0 to π, but the range of θ_l depends on α. Consider the elastic reaction, $1 + 2 \rightarrow 1 + 2$. The quantity α reduces to

$$\alpha = \frac{m_1}{m_2}. \tag{12}$$

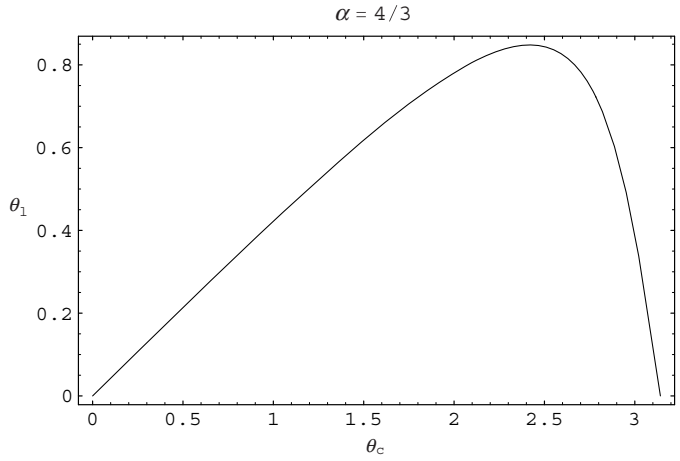

Figure 3. Relation between lab and cm scattering angles.

Goldstein [6, equation (3.110)] reformulates equation (9) as

$$\cos\theta_l = \frac{\cos\theta_c + \alpha}{\sqrt{1 + 2\alpha\cos\theta_c + \alpha^2}}. \tag{13}$$

For $\alpha > 1$, θ_l has a maximum $\theta_{l,\max}$, which is found by differentiating equation (13) with respect to $\cos\theta_c$, setting the derivative equal to zero, and solving for $\cos\theta_l$, to obtain

$$\theta_{l,\max} = \arcsin\left(\frac{1}{\alpha}\right). \tag{14}$$

Solving equation (13) for $\cos\theta_c$ in terms of $\cos\theta_l$ gives

$$\cos\theta_c = -\alpha\sin^2\theta_l \pm \cos\theta_l\sqrt{1 - \alpha^2\sin^2\theta_l} \tag{15}$$

and substituting $\theta_{l,\max}$ from equation (14) gives the corresponding cm angle

$$\theta_c(\text{at } \theta_{l,\max}) = \arccos(-1/\alpha). \tag{16}$$

Equation (15) shows that angle θ_c is a double-valued function of θ_l except at $\theta_{l,\max}$, as seen in figure 3. Differentiating equation (15), and substituting into equation (4), gives the relation between the cm and lab distributions as [7]

$$\frac{\mathrm{d}\sigma}{\mathrm{d}\Omega_l} = \frac{(1 + \alpha^2 + 2\alpha\cos\theta_c)^{3/2}}{|1 + \alpha\cos\theta_c|}\frac{\mathrm{d}\sigma}{\mathrm{d}\Omega_c}. \tag{17}$$

For $m_1 > m_2$ and $\alpha > 1$, the lab distribution in equation (17) has a singularity at the cm angle

$$\theta_{c,\text{sing}} = \arccos\left(\frac{-1}{\alpha}\right). \tag{18}$$

This is the angle given by equation (16), which corresponds to the lab angle given by equation (14), which shows that the singularity occurs at the maximum lab angle:

$$\theta_{l,\text{sing}} = \arcsin\left(\frac{1}{\alpha}\right) \equiv \theta_{l,\max}. \tag{19}$$

The kinematic factor,

$$f(\theta_c) \equiv \left|\frac{\mathrm{d}(\cos\theta_c)}{\mathrm{d}(\cos\theta_l)}\right| = \frac{(1 + \alpha^2 + 2\alpha\cos\theta_c)^{3/2}}{|1 + \alpha\cos\theta_c|}, \tag{20}$$

is plotted in figure 4 for $\alpha = 4/3$, with the singularity prominently displayed at $\theta_c \simeq 2.42$.

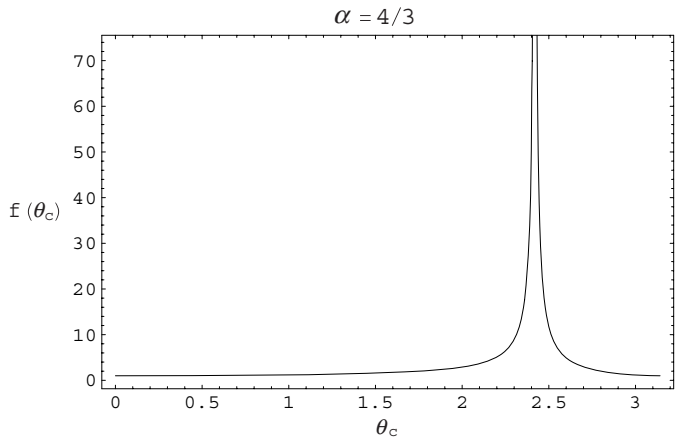

Figure 4. Kinematic factor $f(\theta_c)$.

3.1. Cause of the singularity

The cause of the singularity is made clear by rewriting equation (5) as

$$f \equiv \left| \frac{\mathrm{d}(\cos\theta_c)}{\mathrm{d}(\cos\theta_l)} \right| = \left| \frac{\sin\theta_c}{\sin\theta_l} \frac{\mathrm{d}\theta_c}{\mathrm{d}\theta_l} \right|. \tag{21}$$

The transformation maps cm angles to lab angles. In equation (21), the range of cm angles, $\mathrm{d}\theta_c$, maps to the corresponding range of lab angles, $\mathrm{d}\theta_l$. Furthermore, the ratio $\mathrm{d}\theta_c/\mathrm{d}\theta_l$ increases without bound as the maximum scattering angle is approached (figure 3):

$$\lim_{\theta_l \to \theta_{l,\max}} \frac{\mathrm{d}\theta_c}{\mathrm{d}\theta_l} = \infty. \tag{22}$$

As a result, a range of cm scattering angles near $\theta_{c,\mathrm{sing}}$ is funnelled into a much smaller range of lab angles near $\theta_{l,\max}$. The funnelling effect grows without bound as the lab angle approaches the maximum scattering angle $\theta_{l,\max}$. The funnelling effect is generated by the transformation, and is due entirely to the relative motion of the cm and lab frames.

Equation (15) may be substituted into equation (20) to give f as a function of the lab angle. The kinematic factor $f(\theta_l)$ has two solutions corresponding to the two roots of θ_c. The two solutions f_1 and f_2 are plotted in figures 5 and 6, respectively, with the singularity located at $\theta_{l,\max} \simeq 0.85$ rad.

Both f_1 and f_2 share the same lab angle domain $0 \leqslant \theta_l \leqslant \theta_{l,\max}$, but have different cm angle domains; for f_1: $0 \leqslant \theta_c \leqslant \theta_{c,\mathrm{sing}}$ and for f_2: $\theta_{c,\mathrm{sing}} \leqslant \theta_c \leqslant \pi$. We have shown that the singularity is present in non-relativistic scattering. The following section treats the relativistic case.

4. Relativistic scattering

We derive an expression for f, for relativistic scattering, by finding the transformation between the cm and lab angles. As in the preceding section, f is determined from this transformation. First, note that the element of cross section $\mathrm{d}\sigma$ (figure 1) is perpendicular to the line of relative motion of the projectile and target particles and is, therefore, invariant under Lorentz

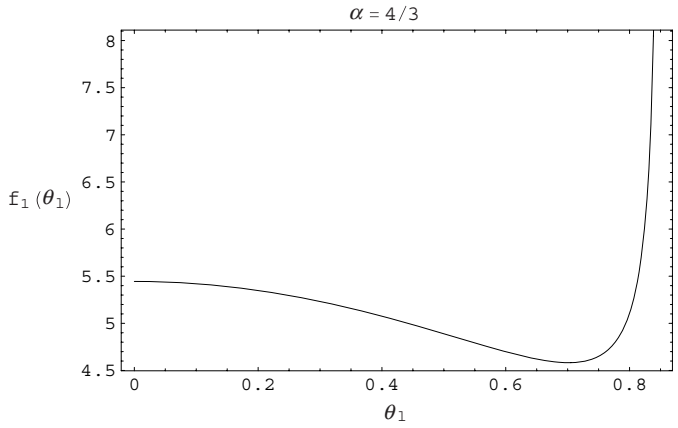

Figure 5. Kinematic factor $f_1(\theta_l)$.

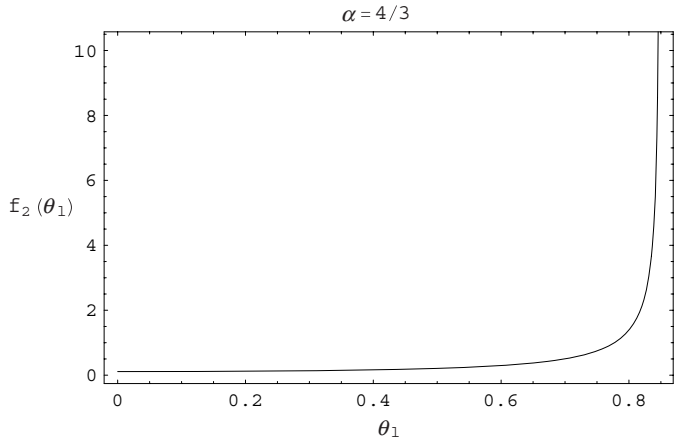

Figure 6. Kinematic factor $f_2(\theta_l)$.

transformation from the cm to the lab frame. Therefore, equation (4) is valid for the relativistic case.

In scattering processes where the speeds of the particles are comparable to the speed of light, a relativistic transformation of velocities is required. The relation between the lab and cm angles is thus obtained in a manner similar to that of section 3, but in this case, we perform a Lorentz, rather than Galilean, transformation of the momentum of the scattered particle from the cm frame to the lab frame. We consider the more general reaction $1 + 2 \rightarrow 3 + 4$, which can be elastic or inelastic, depending on the identities of the final state particles. Let j specify either the final state particle 3 or 4,

$$\tan\theta_{jl} = \frac{\mathbf{p}_{\perp jl}}{\mathbf{p}_{\parallel jl}} = \frac{|\mathbf{p}_{jc}|\sin\theta_{jc}}{\gamma_{cl}(\beta_{cl}E_{jc} + |\mathbf{p}_{jc}|\cos\theta_{jc})}, \tag{23}$$

where $\mathbf{p}_{jl}$ and $\mathbf{p}_{jc}$ are the 3-momenta of particle j in the lab and cm frames, respectively, θ_{jl} and θ_{jc} are the lab and cm scattering angles, E_{jc} is the energy of particle j in the cm frame,

and γ_{cl} and β_{cl} are the usual coefficients of the Lorentz boost between the cm and lab frames, i.e. $\gamma_{cl} \equiv 1/\sqrt{1-\beta_{cl}^2}$ and $\beta_{cl} \equiv v_{cl}/c$. The symbols, $\perp$ and $\parallel$, describe the perpendicular and parallel components of the 3-momentum vectors respectively.

Defining α_{cl} as the relative speed of the cm and lab frames, divided by the speed of particle j in the cm frame, gives

$$\alpha_{jc} = \frac{\beta_{cl}}{\beta_{jc}} \tag{24}$$

$$\beta_{jc} = \frac{|\mathbf{p}_{jc}|}{E_{jc}}, \tag{25}$$

where E is the total energy. Using the result [8, pp 26, 73]

$$\beta_{cl} = \frac{\sqrt{\lambda_{12}}}{s - m_1^2 + m_2^2}, \tag{26}$$

where

$$\lambda_{ij} \equiv \left(s - m_i^2 - m_j^2\right)^2 - 4m_i^2 m_j^2, \tag{27}$$

gives

$$\tan\theta_{jl} = \frac{\sin\theta_{jc}}{\gamma_{cl}(\cos\theta_{jc} + \alpha_{jc})}. \tag{28}$$

See [1, p 402], [4, p 134], [7, p 26], [8, p 42], [31, p 17]. Using the identity $1 + \tan^2\theta_{jl} = 1/\cos^2\theta_{jl}$, equation (28) may be rewritten as

$$\cos\theta_{jl} = \frac{\gamma_{cl}[\cos\theta_{jc} + \alpha_{jc}]}{\sqrt{\gamma_{cl}^2[\cos\theta_{jc} + \alpha_{jc}]^2 + \sin^2\theta_{jc}}}, \tag{29}$$

which may be solved for $\cos\theta_{jc}$ in terms of $\cos\theta_{jl}$, giving

$$\cos\theta_{jc} = \frac{-\alpha_{jc}\gamma_{cl}^2(1 - \cos^2\theta_{jl}) \pm \cos^2\theta_{jl}\sqrt{D}}{1 - \beta_{cl}^2\cos^2\theta_{jl}}, \tag{30}$$

where

$$D \equiv 1 + \gamma_{cl}^2\left(1 - \alpha_{jc}^2\right)\frac{1 - \cos^2\theta_{jl}}{\cos^2\theta_{jl}}. \tag{31}$$

Differentiating equation (29) with respect to $\cos\theta_{jc}$ leads to the kinematic factor

$$\begin{aligned} f(\theta_{jc}) &= \left|\frac{\mathrm{d}(\cos\theta_{jc})}{\mathrm{d}(\cos\theta_{jl})}\right| \\ &= \frac{\left[\gamma_{cl}^2(\alpha_{jc} + \cos\theta_{jc})^2 + \sin^2\theta_{jc}\right]^{3/2}}{|\gamma_{cl}(1 + \alpha_{jc}\cos\theta_{jc})|}. \end{aligned} \tag{32}$$

At low interaction energies, equations (28) and (32) reduce to equations (9) and (20), respectively. Substituting $\cos\theta_{jc}$ from equation (30) into equation (32), f can be expressed in terms of θ_{jl}. Equation (30) shows that θ_{jc} is a double-valued function of θ_{jl}. As in the non-relativistic case, $f(\theta_{jl})$ has two solutions corresponding to the two roots of θ_{jc}.

The denominator of equation (32) shows that f has a singularity at the cm angle:

$$\theta_{jc,\mathrm{sing}} = \arccos\left(\frac{-1}{\alpha_{jc}}\right). \tag{33}$$

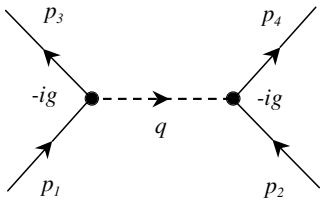

Figure 7. Feynman diagram direct term for reaction $1 + 2 \rightarrow 3 + 4$. The p are the 4-momenta of particles 1 through 4, q is the 4-momentum of the exchange particle and g is the coupling constant.

Substituting equation (33) into equation (29) gives the lab angle at which the singularity occurs:

$$\theta_{jl,\mathrm{sing}} = \arcsin \frac{1}{\sqrt{1 + \gamma_{cl}^2 \left(\alpha_{jc}^2 - 1\right)}}. \tag{34}$$

Equation (33) is identical to equation (18), while equation (34) reduces to equation (14) at low interaction energies, $\gamma_{cl} \sim 1$. The procedure used in section 3 to determine $\theta_{l,\max}$ may also be applied here to demonstrate the equivalence

$$\theta_{jl,\max} = \theta_{jl,\mathrm{sing}}. \tag{35}$$

Plots of the relativistic kinematic factor f are similar to the non-relativistic f, and are not included here. Having shown that the singularity appears in the relativistic factor f, we proceed to illustrate the singularity for the case of inelastic scattering.

5. Application to scattering

The singularity is illustrated with plots of the cm and lab angular distributions for inelastic two-body scattering. The distributions are derived using a scalar (spin zero) quantum field theory [32], in which scalar particles interact by exchanging a single massive scalar exchange particle. Using this one boson exchange (OBE) model, the invariant scattering amplitude $\mathcal{M}$ is found. The square of this amplitude $|\mathcal{M}|^2$ is proportional to the probability that a particle will scatter into a given angle or at a given energy. The distributions are thus proportional to $|\mathcal{M}|^2$, and serve to illustrate how the singularity arises in the transformation of a smooth, finite piece of the cm distribution to the corresponding piece of the lab distribution.

5.1. Lab angular distribution

The interaction of two scalar particles in the reaction, $1 + 2 \rightarrow 3 + 4$, is depicted in figure 7. Applying the Feynman rules of the model [32] to the diagram leads to the amplitude $\mathcal{M}$ expressed in terms of Mandelstam invariants s, t and u:

$$\mathcal{M} = \frac{g_{13x} g_{24x}}{t - m_x^2} + \frac{g_{14x} g_{23x}}{u - m_x^2}, \tag{36}$$

where m_x is the mass of the exchange particle, and

$$s \equiv (p_1 + p_2)^2, \tag{37}$$

$$t \equiv (p_1 - p_3)^2 = (p_2 - p_4)^2, \tag{38}$$

$$u \equiv (p_1 - p_4)^2 = (p_2 - p_3)^2. \tag{39}$$

The amplitude contains two terms. The first term is the direct process and is derived from the diagram in figure 7. The second term is the exchange process and is derived from a similar diagram, but with particles 3 and 4 exchanged. The amplitude is substituted into the invariant distribution, $\mathrm{d}\sigma/\mathrm{d}t$ [9, p 101]:

$$\frac{\mathrm{d}\sigma}{\mathrm{d}t} = \frac{\mathcal{S}}{16\pi\lambda_{12}}|\mathcal{M}|^2. \tag{40}$$

The statistical factor is $\mathcal{S} = 1$, for non-identical final state particles. The cm angular distribution is given in terms of $\mathrm{d}\sigma/\mathrm{d}t$ by [9]

$$\frac{\mathrm{d}\sigma}{\mathrm{d}\Omega_{3c}} = \frac{\mathrm{d}\sigma}{\mathrm{d}t}\frac{\mathrm{d}t}{\mathrm{d}\Omega_{3c}} = \frac{\mathrm{d}\sigma}{\mathrm{d}t}\frac{\mathrm{d}t}{2\pi\,\mathrm{d}(\cos\theta_{3c})}, \tag{41}$$

treating $\mathrm{d}\Omega_{3c}$ as a first-order differential. The factor of 2π in $\mathrm{d}\Omega_{3c}$ comes from integration over $\mathrm{d}\phi$ with the assumption of azimuthal symmetry. The invariant t is expressed in terms of the cm scattering angle by

$$\begin{aligned} t &= (p_4 - p_2)^2 \\ &= m_4^2 + m_2^2 - 2E_4E_2 + 2|\mathbf{p}_4||\mathbf{p}_2|\cos\theta_{4c}, \end{aligned} \tag{42}$$

noting that $\theta_{3c} \equiv \theta_{4c}$. This expression for t, in combination with equation (41), leads to the cm angular distribution [7]:

$$\frac{\mathrm{d}\sigma}{\mathrm{d}\Omega_{3c}} = \frac{\mathcal{S}}{64\pi^2 s}\sqrt{\frac{\lambda_{34}}{\lambda_{12}}}\left[\frac{g_{13x}g_{24x}}{t - m_x^2} + \frac{g_{14x}g_{23x}}{u - m_x^2}\right]^2, \tag{43}$$

where g_{ijk} are the coupling constants among particles i, j, k, and

$$t = m_2^2 + m_4^2 - \frac{1}{2s}\sqrt{\left(\lambda_{12} + 4sm_2^2\right)\left(\lambda_{34} + 4sm_4^2\right)} + \frac{1}{2s}\sqrt{\lambda_{12}\lambda_{34}}\cos\theta_{3c} \tag{44}$$

$$u = \sum_{i=1}^{4} m_i^2 - s - t. \tag{45}$$

Finally, applying the angle transformation equation (30) and the relativistic kinematic factor in equation (32) to equation (43) leads to the lab angular distribution

$$\frac{\mathrm{d}\sigma}{\mathrm{d}\Omega_{3l}} = \frac{4m_2 s}{\sqrt{\lambda_{12}\lambda_{34}}}\frac{|\mathbf{p}_{1l}||\mathbf{p}_{3l}|}{|E_{1l} + m_2 - \frac{|\mathbf{p}_{1l}|}{|\mathbf{p}_{3l}|}E_{3l}\cos\theta_{13l}|}\frac{\mathrm{d}\sigma}{\mathrm{d}\Omega_{13c}}, \tag{46}$$

where

$$|\mathbf{p}_{jl}| \equiv \sqrt{E_{jl}^2 - m_j^2}. \tag{47}$$

In this form, the lab angular distribution is given in terms of E_{3l}, the energy of particle 3 in the lab frame. For computational purposes, both E_{3l} and $\mathrm{d}\sigma/\mathrm{d}\Omega_{13c}$, the latter of which contains t, are written as functions of θ_{3l} and the interaction energy E_{1l} by using

$$s = m_1^2 + m_2^2 + 2E_1m_2 \tag{48}$$

$$t = m_4^2 - m_2^2 + 2m_2(E_{3l} - E_{1l}), \tag{49}$$

and

$$\begin{aligned} E_{3l} = \frac{ab}{D} &\pm \frac{\sqrt{E_{1l}^2 - m_1^2}\cos(\theta_{3l})}{D} \\ &\times\sqrt{a^2 - m_3^2\left[b^2 - \left(E_{1l}^2 - m_1^2\right)\cos^2(\theta_{3l})\right]} \end{aligned} \tag{50}$$

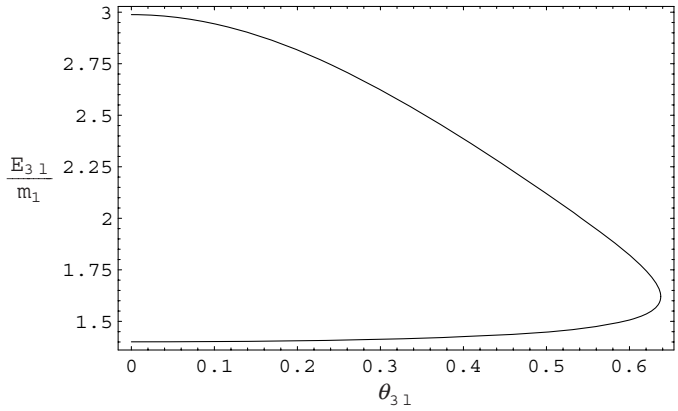

Figure 8. Lab energy $E_{3l}(\theta_{3l})$.

with

$$D \equiv b^2 - \left(E_{1l}^2 - m_1^2\right)\cos^2(\theta_{3l}) \tag{51}$$

$$a \equiv \frac{s + m_3^2 - m_4^2}{2} \tag{52}$$

$$b \equiv E_{1l} + m_2. \tag{53}$$

Equation (50) shows that, in general, for a single value of lab angle θ_{3l}, the energy E_{3l} has two roots. These roots correspond to the two roots of the cm angle θ_{3c} given by equation (30). The two roots of E_{3l} are plotted together in figure 8, forming respectively the upper and lower parts of the curve, and joining at $\theta_{3l,\max} \simeq 0.64$ rad. This plot corresponds to the inelastic reaction described in section 5.2. The two values of E_{3l} signify that particles of two different energies are scattered into the angle θ_{3l}. The presence of two energy roots requires that the lab angular distribution be expressed as the sum of two terms, each a function of one of the energy roots:

$$\frac{\mathrm{d}\sigma}{\mathrm{d}\Omega_{3l}} = \frac{\mathrm{d}\sigma}{\mathrm{d}\Omega_{3l}}(E_{3l,\mathrm{root1}}) + \frac{\mathrm{d}\sigma}{\mathrm{d}\Omega_{3l}}(E_{3l,\mathrm{root2}}). \tag{54}$$

We have determined expressions for the cm and lab angular distributions. In the following section, these are plotted for a particular inelastic reaction defined by the masses of the interacting particles and the energy of interaction.

5.2. Analysis of inelastic scattering

The reaction, $1 + 2 \to 3 + 4$, describes an inelastic scattering process when one or both of the final state particles differ from the initial state particles. We define our inelastic process by setting $m_1 = m_2 = m_4$, and $m_3/m_1 = 4/3$. Particle 1 is treated as the projectile, while particle 2 is the stationary target. Initial state particles 1 and 2 are identical. We set the mass of the exchange particle by $m_x/m_1 = 1/7$. The energy of the projectile E_{1l} is the interaction energy, and we set it to $E_{1l} = 3m_1$, sufficient to produce the final state particles. For correspondence to a real process, the mass ratios are chosen to be approximately the same as the mass ratios occurring in the well-known reaction $P + P \to P + \Delta$ modelled as a one pion exchange

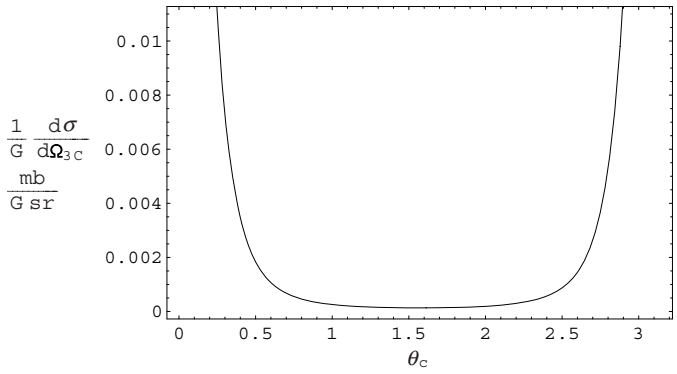

Figure 9. Angular distribution in the cm frame.

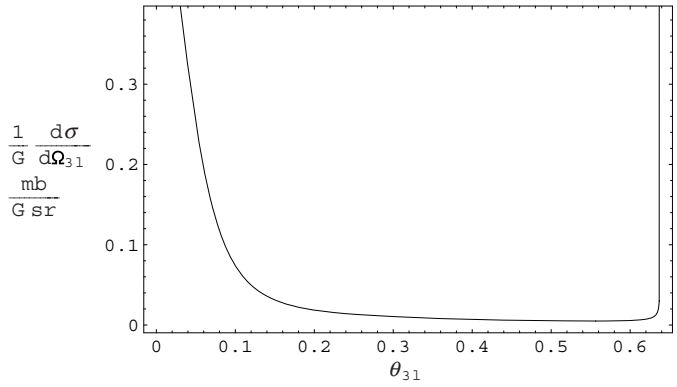

Figure 10. Angular distribution in the lab frame.

process, in which two protons (P) exchange a pion to produce a delta baryon (Δ). In this process, the mass ratios are $m_\Delta/m_P \simeq 4/3$ and $m_\pi/m_P \simeq 1/7$, where m_Δ is the resonance mass, m_P is the proton mass and m_π is the mass of the exchange pion.

The cm and lab distributions are plotted in figures 9 and 10, respectively. The plots are normalized to a combined coupling factor $G = g_{13x}^2 g_{24x}^2 = g_{14x}^2 g_{23x}^2$. The 'horns' in the cm angular distribution located at $\theta_{3c} = 0$ and $\theta_{3c} = \pi$ are finite, demonstrated by evaluating $t(\theta_{3c} = 0)$ and $t(\theta_{3c} = \pi)$ using equation (44), and substituting into equation (43). Both horns map to the single finite horn located at $\theta_{3l} = 0$ in the lab angular distribution. These horns arise from preferential forward scattering, and they are distinguished from the infinite horn at $\theta_{3l,\max} \simeq 0.64$ rad, which arises from the aforementioned funnelling effect near $\theta_{3l,\max}$ (see subsection 3.1). The corresponding cm angle is $\theta_{3c,\mathrm{sing}} \simeq 2.38$ rad. Note how the smooth, finite portion of the cm angular distribution around $\theta_{3c,\mathrm{sing}}$ maps to the infinite horn in the lab angular distribution.

For the inelastic scattering process considered in this section, the total cross section σ is finite, which is demonstrated most directly by integrating equation (40) over the allowed range of t, with u defined in terms of t in equation (45),

$$\sigma = \int_{t(\theta_c=0)}^{t(\theta_c=\pi)} \frac{\mathrm{d}\sigma}{\mathrm{d}t}\,\mathrm{d}t. \tag{55}$$

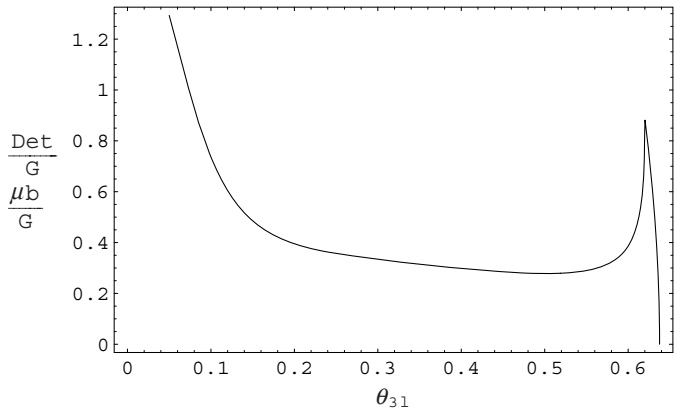

Figure 11. Detector *partial* cross section.

The total cross section may also be found by integrating $\mathrm{d}\sigma/\mathrm{d}\Omega$:

$$\sigma = \int_{\phi=0}^{\phi=2\pi} \int_{0}^{\theta_{l,\max}} \frac{\mathrm{d}\sigma}{\mathrm{d}\Omega_l}\, \mathrm{d}\Omega_l. \tag{56}$$

The total cross section has units of area, and represents the cross sectional area of the target particle as seen by the projectile particle. This cross sectional area is perpendicular to the line of relative motion of the projectile and target particles, and it is, therefore, invariant under Lorentz transformation from the cm frame to the lab frame. The two integrals in equations (55) and (56) must therefore be equivalent. The above integration of the lab angular distribution $\mathrm{d}\sigma/\mathrm{d}\Omega_l$ over the range of lab scattering angles involves integration over the singularity. Since the total cross section is finite, integration over the singularity can make only a finite contribution to the total cross section, and it can make only a finite contribution to the *partial* cross section determined by integration over a small range of angles about $\theta_{l,\max}$. Such a small range of angles is subtended by a macroscopic detector. An idealized detector of infinitesimal angular width 'sees' the bare singularity, but a macroscopic detector of finite width sees a finite bump in the angular distribution in the vicinity of $\theta_{l,\max}$.

The 'detector' plot in figure 11 shows the partial cross section measured by a ring-shaped detector (the ring labelled dΩ in figure 1) of a varying solid angle $\Delta\Omega = 2\pi \sin\theta_{3l}\Delta\theta_{3l}$, but fixed width $\Delta\theta_{3l} = 17.45\,\mathrm{mrad} = 1^\circ$, as the detector is positioned over a continuous range of angles $0 < \theta_{3l} < \theta_{3l,\max}$. The singularity in the lab angular distribution (figure 10) produces the sharp peak in the detector cross section (figure 11) near $\theta_{l,\max}$.

6. Conclusions

Two-body scattering theory gives expressions for the cm and lab angular distributions. For the inelastic reaction considered, the cm angular distribution has sharp but finite peaks at the extremities of the scattering range $\theta_c = 0$ and $\theta_c = \pi$, and is smooth throughout, having no singularities over the range $0 \leqslant \theta_c \leqslant \pi$. The lab angular distribution is related to the cm angular distribution by a Galilean or Lorentz transformation. This paper highlights the transformation by demonstrating that a singularity resides in the kinematic factor generated by the transformation from the cm to lab frame. This factor multiplies the cm angular distribution to produce the lab angular distribution. The singularity is caused by the funnelling of a range of

cm scattering angles to a much smaller range of lab angles. The funnelling effect grows as the lab angle approaches the maximum scattering angle $\theta_{l,\max}$. In the limit as θ_l approaches $\theta_{l,\max}$, the ratio of the ranges goes to infinity. The singularity is seen to be a purely kinematic effect, present even for cases of low relative speeds of the interacting particles or, equivalently, cases of non-relativistic motion between the cm and lab frames. The funnelling effect highlights how the angular distribution is shaped by relative motion.

Transformation of angular distributions from the centre of momentum to the lab frame is often studied at the non-relativistic level by undergraduate and graduate students in courses on classical and quantum mechanics. The detailed study of the singularity is often not considered. However, advanced students may well come across the singularity if they pursue the problem fully. Naturally, both students and teachers alike will want to know about the relativistic extension, which our paper provides in conjunction with the non-relativistic treatment.

Acknowledgments

John Norbury thanks Professor J D Jackson for very helpful correspondence. The authors also thank Rachel Nasto and Ryan Norman for verifying some results.

References

[1] Jackson J D 1972 *Classical Electrodynamics* 1st edn (New York: Wiley)
[2] Schiff L I 1949 *Quantum Mechanics* 1st edn (New York: McGraw-Hill)
[3] Baldin A M, Goldanskii V I and Rozental I L 1961 *Kinematics of Nuclear Reactions* (Oxford: Oxford University Press)
[4] Newton R G 1982 *Scattering Theory of Waves and Particles* 2nd edn (New York: Springer)
[5] Marion J B 1970 *Classical Dynamics of Particles and Systems* 2nd edn (New York: Academic)
[6] Goldstein H, Poole C and Safko J 2002 *Classical Mechanics* 3rd edn (San Francisco: Addison-Wesley)
[7] Joachain C J 1983 *Quantum Collision Theory* (Amsterdam: North-Holland)
[8] Byckling E and Kajantie K 1973 *Particle Kinematics* (New York: Wiley)
[9] Ho-Kim Q and Xuan Yem P 1998 *Elementary Particles and their Interactions* (New York: Springer)
[10] Galindo A and Pascual P 1990 *Quantum Mechanics II* (New York: Springer)
[11] Das A and Melissinos A C 1986 *Quantum Mechanics* (New York: Gordon and Breach)
[12] Mandl F 1957 *Quantum Mechanics* (London: Butterworths Scientific Publications)
[13] Park D 1964 *Introduction to Quantum Mechanics* (New York: McGraw-Hill)
[14] Desloge E 1989 *Classical Mechanics* vol 1 (Malabar, FL: Krieger)
[15] Bohm D 1951 *Quantum Theory* (New York: Prentice-Hall)
[16] Farina J 1973 *Quantum Theory of Scattering Processes* (Oxford: Pergamon)
[17] Sitenko A 1971 *Lectures in Scattering Theory* (Oxford: Pergamon)
[18] Barger V and Kline D B 1969 *Phenomenological Theories of High Energy Scattering* (New York: Benjamin)
[19] Dedrick K G 1962 Kinematics of high energy particles *Rev. Mod. Phys.* **34** 429–42
[20] Chow T L 1995 *Classical Mechanics* (New York: Wiley)
[21] Hagedorn R 1963 *Relativistic Kinematics* (New York: Benjamin)
[22] Krane K S 1988 *Introductory Nuclear Physics* (New York: Wiley)
[23] Pilkuhn H M 1979 *Relativistic Particle Physics* (New York: Springer)
[24] Mathews P M and Venkatesan K 1978 *A Textbook of Quantum Mechanics* (New York: McGraw-Hill)
[25] Rossberg K 1983 *A First Course in Analytical Mechanics* (New York: Wiley)
[26] Barford N C 1973 *Mechanics* (New York: Wiley)
[27] Kibble T W B 1973 *Classical Mechanics* 2nd edn (New York: Wiley)
[28] Taylor J R 1972 *Scattering Theory* (New York: Wiley)
[29] Cheng D C and ONeill G K 1979 *Elementary Particle Physics* (Reading, MA: Addison-Wesley)
[30] Segre E 1977 *Nuclei and Particles* 2nd edn (Reading, MA: Benjamin-Cummings)
[31] Leon M 1973 *Particle Physics: An Introduction* (New York: Academic)
[32] Griffiths D J 1987 *Introduction to Elementary Particles* (New York: Wiley)